Methods for Improving Quantitation of Putamen Uptake Constant of FDOPA in PET Studies

Dan-Chu Yu, Sung-Cheng Huang, Scott T. Grafton, William P. Melega, Jorge R. Barrio, John C. Mazziotta and Michael E. Phelps

Division of Nuclear Medicine, Department of Pharmacology, Department of Neurology, Laboratory of Nuclear Medicine, UCLA School of Medicine, University of California at Los Angeles, Los Angeles, California

To estimate the striatal uptake constant of [^{18}F]-L-6-fluorodopa (FDOPA) in humans, we studied two methods that can account for the image resolution and the background level of FDOPA. These two methods utilize information obtained from multiple ROIs varying in size around the putamen and from profiles crossing the middle of the putamen. The estimation of the uptake constant was based on a model of one-dimensional activity variation. Simulated data were used to evaluate the adequacy of these two methods. Parametric images of FDOPA uptake constants were generated using Patlak analysis for five studies in normals and were then analyzed with the two methods. Results from the simulated data indicated a good agreement between the estimated values and the true simulated values. Results from studies in normals show stable estimates of the FDOPA uptake constant that are not affected by image resolution. The two methods were not sensitive to the misplacement of ROIs and profiles.

J Nucl Med 1993; 34:679–688

Fluorine-18-L-6-fluorodopa (FDOPA) has been used in PET to examine the integrity of the presynaptic doparminergic system. In normal subjects, FDOPA uptake has been shown to be higher in the caudate and putamen than in other cerebral tissues (1–4). The caudate and putamen contain aromatic amino acid decarboxylase (AAAD) that converts FDOPA to [^{18}F]-L-6-fluorodopamine (Fdopamine) which is retained in neurons (5). The uptake of FDOPA has also been found to decrease in patients with Parkinson's disease and in subjects exposed to 1-methyl-4-phenyl-1,2,3,6-tetrahydropyridine (MPTP) (6–10). Therefore, the rate of uptake of FDOPA is believed to be a useful index for measuring abnormalities in the presynaptic dopaminergic system.

After FDOPA injection, the tracer can be metabolized in plasma into 3-O-methyl-FDOPA (OMFD) (11), which can cross the blood-brain barrier (BBB). Thus, the total tissue radioactivity measured by PET is partially due to OMFD. This complicates the interpretation of FDOPA data. A model approach that can account for OMFD has been developed to analyze FDOPA PET data (3,4). With this approach, the transport rate constant across the BBB and the decarboxylation rate constant for FDOPA in striatum can be separately estimated. The Patlak analysis method (12,13) has also been used to estimate the uptake constant (K_3) of FDOPA in striatum (2). However, in the estimation of the FDOPA uptake constant, various error sources, including the small size of the striatal structure or the inaccurate definition of the region of interest (ROI), could affect the accuracy and reliability of the results (14–16).

In PET images, small structures such as the caudate and putamen, which are smaller than two times the full width at half maximum (FWHM) of the scanner system, will have an apparent depression of its radioactivity concentration, due to the partial volume effect. The recovery coefficient (RC) has been introduced as the ratio of the measured over the true concentration to correct for the partial volume effect (14,16). However, it is not easy to use the RC in realistic situations because it depends on background levels (17) and requires knowledge of the true object size.

In order to extract the radioactivity concentration in a small tissue structure, e.g., the putamen, a ROI is usually drawn over the object of interest on the PET image and the average counts within the ROI are regarded as the concentration contained in the structure. For the putamen, the size of the ROI must be small to ensure that the radioactivity concentration within the ROI is uniform. Because of uncertainty about the anatomical border and the partial volume effect, the usual criterion of defining a ROI along the boundary of the putamen on a PET image cannot accurately measure concentration. Various methods have been used by many investigators to avoid partial

volume effects and ROI size problems. For example, Gjedde et al. (*18*) used MRI to assist in defining a ROI for the striatum, but not for correcting partial volume effects. Martin et al. (*2*) used a large ROI (12 cm^2) that enclosed the entire striatum to calculate the uptake constant in terms of the whole striatum instead of a unit weight of the striatal tissue. Their method resulted in a very large K_3 value per striatum, possibly due to the inclusion of a nonzero background uptake in the adjacent tissue. Eidelberg et al. (*19*) used the average value of the upper 15% ROI pixel values (*20*). This measurement was expected to be sensitive to high statistical noise levels and the method did not remove the dependency on image resolution.

FDOPA uptake in the striatum has been studied by different groups. However, due to the different PET systems employed and the resolution dependence of quantitation methods they adopted, results cannot be cross-compared among different investigators (*17*). In this study, we investigate a profile method and a multiple ROI method to provide resolution-independent and reliable estimates of striatal FDOPA uptake constants. These two methods are based on the concept that utilize more information on spatial distribution of true activity and can therefore provide a more accurate estimate of the FDOPA uptake constant than the single ROI method.

METHOD

Theory

In order to accurately estimate the uptake constant of FDOPA in the putamen, factors such as object size, imaging resolution and background level (i.e., uptake constant in adjacent tissue regions) have to be considered. To simplify the problem, we first assume that: (1) the background level is constant; (2) the structure of interest has a uniform concentration level; (3) there is no variation along the axial direction; (4) the structure is long in one direction (i.e., there is little variation along that direction); thus, the structure can be regarded as a one-dimensional object (for example, an infinite long bar); and (5) the line-spread function of the PET imaging system has a Gaussian shape. With these assumptions and approximations, analytical functions for the image values (as a function of distance) and the ROI values (as a function of ROI size) can be derived similar to what has been done for the myocardium (*21*), as shown in the following example.

Let C_p and C_b represent the uptake constants of the putamen and background (i.e., $(K_3)_{putamen}$ and $(K_3)_{background}$), respectively, in the simulation and w is the width of the structure as shown in Figure 1. Based on the assumptions listed above, the imaged activity level (Act(x)) at a distance x from the center of the object can be expressed as:

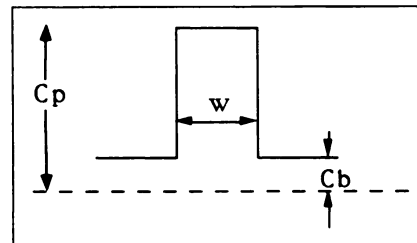$$Act(x) = \frac{(C_p - C_b)}{\sqrt{2\pi s^2}} \int_{-\frac{w}{2}}^{\frac{w}{2}} e^{-\frac{(x-t)^2}{2s^2}} dt + C_b$$

FIGURE 1. A sketch diagram of the activity distribution assumed for the methods investigated in this study.

$$= \frac{(C_p - C_b)}{\sqrt{2\pi s^2}} \int_{lb}^{rb} e^{-u^2} du + C_b$$

$$= \frac{(C_p - C_b)}{2} [ERF(rb) - ERF(lb)] + C_b, \quad Eq. 1$$

where $ERF(u) = (2/\sqrt{\pi}) \int_0^u e^{-t^2}$, dt is the mathematical error function (*22*) and s is determined by the FWHM of the scanner resolution (s = FWHM/2.355), lb = $(x - w/2)/(\sqrt{2}s)$, rb = $(x + w/2)/(\sqrt{2}s)$.

If a rectangular ROI with a width d centered around the object is used, the ROI value (ROI(d)) can be expressed as:

$$ROI(d) = \int_{-\frac{d}{2}}^{\frac{d}{2}} Act(x)dx$$

$$= (C_p - C_b) \int_{-\frac{d}{2}}^{\frac{d}{2}} ERF\left(\frac{x + \frac{w}{2}}{\sqrt{2}\ s}\right) dx + C_b \times d. \quad Eq. 2$$

Equation 1 is used to fit the profile across the middle part of the putamen to estimate w, C_p, C_b and the center of the object. This will be referred to as the profile method. Alternatively, Equation 2 is used to fit the ROI values obtained from ROIs of different sizes (different width) to estimate the values of w, C_p and C_b. This is referred to as the multiple ROI method. For realistic objects in real situations, the assumptions about the structural shape and its axial variation are not rigorously valid. Deviation from the assumption of an infinitely long bar with no axial variation is, however, expected to cause the imaged object's boundaries to be more blurry, equivalent to having a lower image resolution. If this is true, then the FWHM value used in Equations 1 and 2 is expected to be larger than the normal value of image resolution. We have investigated the validity of this equivalency with computer simulation described in the following section and have determined the proper FWHM values that would provide the correct estimate of C_p.

Simulation

Noise-free images and images with a noise level comparable to that of FDOPA PET parametric images were generated by computer simulation. Structures of three different shapes (rectangle, ellipse and nonrectangular polygon) were simulated. The rectangle was 3.4 × 1.1 cm, with its area and width similar to those of a transaxial cut of the putamen. The ellipse had its
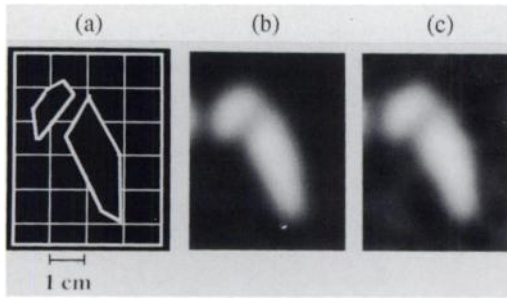
FIGURE 2. (a) Outline of a simulated polygon that imitated the shape of caudate and putamen in PET images. The left striatum, which is symmetrical to this sketch, was also simulated on the same image. (b) Simulated noise-free image generated from the polygon shown in (a) with an imaging resolution of 0.74 cm FWHM. (c) Simulated image (0.74 cm FWHM) with a noise level comparable to that of a parametric image of the FDOPA uptake constant in normal PET studies.
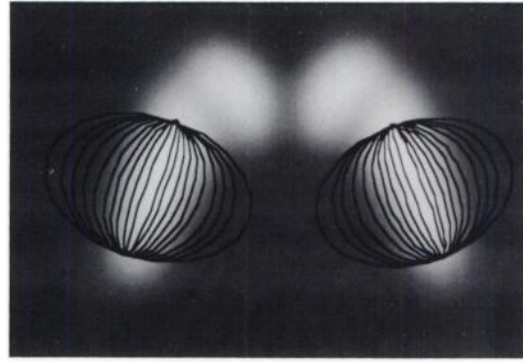

FIGURE 3. A set of ROIs drawn over the putamen in a normal subject for application of the multiple ROI method. All ROIs are elliptical in shape and have the same long-axis.

long-axis equal to 3.4 cm and its short-axis equal to 1.1 cm. The polygon closely imitated the shapes of the caudate and putamen as shown in Figure 2. A mirror image of the polygon was used to simulate the structures on the lefthand side. In the simulations, the activity of these structures that represents the uptake constant of putamen (C_p) was assumed to be six times the background level (i.e., $C_b = \frac{1}{6}C_p$) to simulate real FDOPA data in normal studies. To examine conditions in pathological cases, the simulations were repeated three more times with three other C_p levels ($C_p = 4C_b$, $3C_b$ and $2C_b$).

Each sinogram consisted of 160 angular views and 128 linear samples with an intrinsic resolution of 4.8 mm (FWHM) and sampling distance of 3.14 mm. Pseudo-random noise was added to the sinograms to simulate a noise level (45% s.d. in the nonstriatal area when the Shepp filter was used) comparable to that in a real parametric image of the FDOPA uptake constant. Each sinogram was then reconstructed four times using four different filters: Shepp-Logan filter with cutoff frequency at the Nyquist frequency; Hanning filter with cutoff at 1.0, 0.7 and 0.5 of the same Nyquist frequency to give images with spatial resolutions of 0.56, 0.74, 0.94 and 1.24 cm FWHM, respectively. Cross-sectional profiles across the structures were obtained from these images and elliptical ROIs of various sizes (to be described later) were applied to these images.

The noise-free simulation data were used to determine the equivalent FWHM for different structural shapes and to examine the adequacy of Equations 1 and 2 for describing the data. In this determination, the profile data and multiple-ROI data were curve fitted by Equations 1 and 2, respectively, with C_p fixed at its true value (6) to estimate FWHM, width and C_b. The simulated data with noise were generated with five different noise realizations. They were used to validate the two proposed methods and to test their stability.

PET Data

Five normal subjects were studied. Each subject was given 250 mg carbidopa orally 1 hr before the injection of FDOPA (5 mCi). A dynamic PET scan was initiated immediately after tracer administration and a total of 18 frames were acquired on a Siemens CTI 831-08 PET scanner (Siemens Gammasonics, Inc., Des Plaines, IL) with a scanning sequence of 6 × 0.5, 4 × 3, 5 × 10 and

3 × 20 min. Twenty arterial blood samples were taken at gradually increasing intervals, with 12 samples in the first 2 min. Five to six blood samples (at 5, 10, 20, 30, 60 and 120 min) were biochemically assayed by HPLC to give the percent composition of FDOPA, OMFD and other metabolites at those time points. The FDOPA plasma time-activity curve was generated from the total plasma ^{18}F activity curve and the biochemical assayed data by a modeling approach (4). Photon attenuation was corrected either by measured (in two studies) or calculated (in three studies) correction methods (23). PET images (128 × 128, pixel width = 0.157 cm) of four different resolutions were reconstructed for each scan with the same four filters used for the simulation data.

The FDOPA uptake constant (K_3) was calculated pixel-by-pixel utilizing the Patlak graphical analysis method to generate the parametric image for the image plane that had the highest contrast between the putamen and background. Each pixel value of the parametric image represents the slope of the Patlak plot (K_3). In the Patlak analysis, the output function was the dynamic image pixel values from 12 to 120 min. To reduce the contribution due to OMFD, each pixel of the images was subtracted by an image value of the cerebellum (a reference tissue region which is devoid of dopaminergic terminals) at the corresponding scan time. The cerebellar image value was obtained from ROIs on the cerebellum (4). The validity of the subtraction was based on the assumption that the transport of OMFD across the BBB was similar for all cerebral tissues (28). The input function used in the Patlak analysis was the plasma FDOPA time-activity curve.

Data Analysis

Multiple ROI Definition. A series of ROIs varying in size from 0.4 cm² to 10 cm² (Fig. 3) were defined on the parametric images of FDOPA uptake constant as well as on the computer simulated images. Each set of ROIs consisted of 8–10 regions. For each subject, three sets of elliptical ROIs with three different long axes that are aligned with the center line of the putamen (Fig. 3) were defined to examine the sensitivity of the method to the ROI shape. Each set of ROIs was also shifted by one and two pixels horizontally to test the sensitivity of the multiple ROI method to the misplacement of ROIs. Elliptical ROIs were used instead of rectangles because they are more commonly used in practice and are closer to the shape of the putamen. This deviation from the theory is expected to increase the equivalent

TABLE 1
FWHM, Background Uptake and Structural Width Estimated by the Profile and Multiple ROI Methods from Noise-Free Simulated Data

Shape of structure	True FWHM (cm)	Profile				Multiple ROI			
		Shepp 1 (0.56)*	Hann 1 (0.74)	Hann 0.7 (0.94)	Hann 0.5 (1.24)	Shepp 1 (0.56)	Hann 1 (0.74)	Hann 0.7 (0.94)	Hann 0.5 (1.24)
Rectangle	FWHM	0.56	0.75	0.94	1.24	0.69	0.90	1.13	1.53
	C_b (1)	0.97	0.97	0.97	0.96	1.05	1.04	1.01	0.92
	Width (1.1)	1.09	1.09	1.09	1.11	1.27	1.27	1.27	1.30
Ellipse	FWHM	0.56	0.75	0.94	1.24	0.73	0.93	1.20	1.64
	C_b (1)	0.97	0.97	0.97	0.96	1.05	1.06	1.01	1.16
	Width (1.1)	1.08	1.07	1.06	1.06	1.23	1.22	1.20	1.18
Polygon	FWHM	0.61	0.80	1.01	1.36	0.69	0.89	1.11	1.49
	C_b (1)	0.98	1.00	1.02	1.02	1.21	1.21	1.22	1.19
	Width (1.15)	1.17	1.15	1.13	1.13	1.18	1.14	1.13	1.12

*Numbers in parentheses represent true values. The true FWHM for each reconstruction filter is based on the image profile of a reconstructed line source.

FWHM value in Equation 2, which is similar to the effects for realistic object shapes discussed earlier.

Profile Data. Profiles of 30 pixels long (4.71 cm) along the horizontal direction of the image and crossing the center regions (near one-third of the length from the anterior end) of the putamen were obtained for each computer simulated image and for each parametric image of the FDOPA uptake constant. The average of three consecutive profiles of the parametric images was used in the curve fitting.

Comparison with Single ROI and Thresholding Methods. A single ROI was defined on the parametric image reconstructed with Hanning filter at a cutoff frequency equal to the Nyquist frequency. ROIs were drawn manually around the putamen (size = 2.0–2.5 cm²) and then applied to the other parametric images of different resolutions. For the percent thresholding method (20), the ROI value was the average of the pixel values within 15% of the maximum pixel value within the entire putamen area. The total area for the pixels above the upper 15% threshold (above 0.85 × maximum pixel value) in the putamen ROI varied from 0.7 cm² for the highest resolution (Shepp-Logan filter at a cutoff of 1) to 2.7 cm² for the lowest resolution (Hanning filter at a cutoff of 0.5). The mean and standard deviation of the ROI values were calculated and compared to those of the profile and multiple-ROI methods. The correlation between the single ROI method and the two new methods was also examined.

Regression Analysis. Profile and multiple-ROI measurements were fitted by Equation 1 and Equation 2, respectively. For the noise-free simulation data, C_p was fixed to the true value to determine the appropriate FWHM value to use. The FWHM so determined for the polygon was then applied to the noise-added simulation data and to the real PET data to estimate the putamen and background uptake constants and structural width. All data fittings were performed using the least squares regression routine in the BLD software package (24).

RESULTS

Computer Simulated Data

Two images of the simulated putamen are shown in Figures 2b and 2c. The simulated putamen and caudate were generated according to the polygon shown in Figure 2a. ROI values for the simulated noise-free images were obtained from the set of ROIs shown in Figure 3 by placing them on the images of four different image resolutions. The ROI values so obtained were found to fit well by Equation 2 (correlation coefficient (c.c.) = 0.99). The image profiles across the middle of the simulated putamen (noise-free) were also found to fit well by Equation 1 (c.c. = 0.99). The good fittings indicate that the functional forms of Equations 1 and 2 can describe the data well.

Table 1 summarizes the estimation results for both the profile and multiple ROI methods. Estimates of C_b and width were generally close to the true values. As expected, the estimated FWHM values in Table 1 were shown to be larger than its true value. The estimated FWHM values for the polygon shape were used for estimating C_p (for the noise-added simulation data) and K_3 for the PET studies.

Figure 2c shows an image reconstructed from computer simulated data with a noise level similar to that of the real PET FDOPA images. The image profiles obtained from the simulated images at four resolutions and their fitting results are shown in Figure 4a. The ROI values are shown in Figure 4b along with the fitting results from Equation 2. The results from applying the profile and multiple ROI methods for estimating the values of C_p, C_b are shown in Figure 5. It includes the estimates for the four different imaging resolutions. The estimates of C_p and C_b are shown independent of the imaging resolution

and are close to the true values. Table 2 shows the results when the contrast between the putamen and its background is lower. To compare the performance of the two proposed methods to that of the single ROI and thresholding methods, the estimated C_p by different methods at four different resolutions are shown in Figure 6.

PET Data

Figure 7 shows a set of parametric images at four different image resolutions of the FDOPA uptake constant K_3 generated from a dynamic sequence of PET images of a typical human FDOPA study. The pixel value represents the FDOPA uptake constant at that location. A higher value for the caudate and putamen regions as compared to the background level is clearly shown. These images also show a strong dependency of the image noise level on image resolution. The profiles and ROI values from a set of these images are shown in Figure 8 together with their fitting results from Equations 1 and 2.
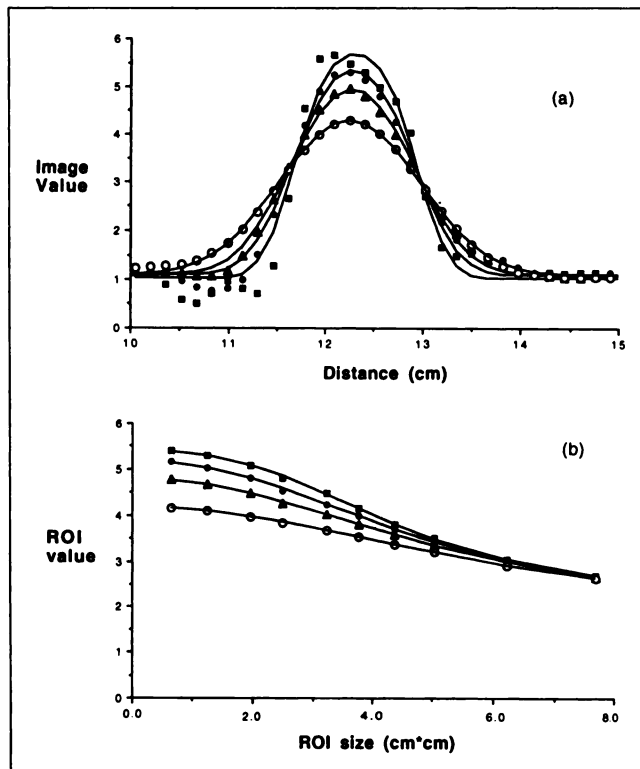

FIGURE 4. (a) Profile across the middle of the simulated putamen in images with noise level similar to the PET FDOPA studies. The profiles are the average of three adjacent profiles (three pixels). Different symbols correspond to images from different reconstruction filters (square: Shepp 1; circle: Hann 1; triangle: Hann 0.7; unfilled circle: Hann 0.5). The solid curves are fitting results of the data by Equation 1. (b) ROI values as a function of ROI size on the noise-added images of the simulated structure of Figure 2a. The curves are fitting results by Equation 2. Different symbols correspond to the four different imaging resolutions as described in (a). Note that the ROI values from the images of all four resolution were lower than the true value (= 6) even with a very small ROI.
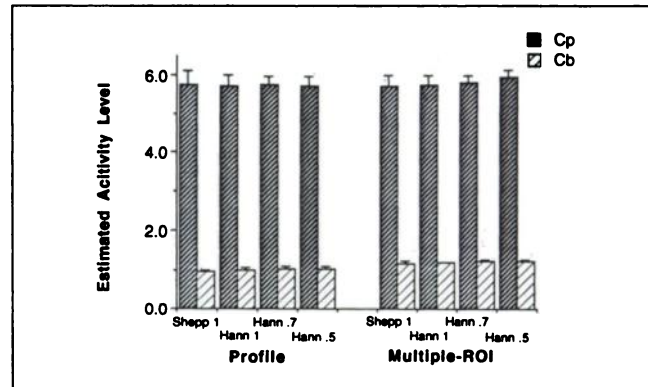

FIGURE 5. Estimates of C_p and C_b by the two new methods for four different resolutions from the computer simulated images. The error bar are the standard deviations of the estimates in five noise realizations.

The measured ROI values are closely related to ROI size and image resolution. Figure 9 shows the estimates of $(K_3)_{putamen}$ and $(K_3)_{background}$ by the new methods as a function of image resolution.

Sensitivity of the K_3 estimates to ROI misplacement, ROI dimensional change, and profile locations were evaluated and the results are shown in Table 3. The estimates were not sensitive to these factors except for a large misplacement of ROI (0.314 cm). For the profile method, moving the profile within the range of 1 cm near the center part of the putamen did not affect the $(K_3)_{putamen}$ estimate significantly.

DISCUSSION

The small size (relative to imaging resolution) of individual cerebral structures is a major problem for accurate quantitative analysis of neurologic PET data. Consistent and reliable results are difficult to obtain if quantitative analysis is strongly dependent on image resolution, object size and the ROI used. In this study, we have demonstrated that the profile and multiple ROI methods are able to correct for the resolution-dependent partial volume effect on the measurements of putamen FDOPA uptake constant without requiring additional anatomical information from CT or MR scans. The two methods are also less sensitive in defining ROIs than the conventional method of using a single ROI.

As shown in Figures 4 and 8, the data obtained from the profiles and multiple ROIs can be well described by the fitting equations that are based on the assumption of one-dimensional variation of the activity distribution. Rigorously, only long rectangular structures satisfy the assumption. However, by proper definition of the ROIs or careful selection of the profile location and appropriate adjustment of the FWHM in the fitting equation, the results can be well approximated by the relationship based on one-dimensional variations. As shown in Table 1, the magnitude of the adjustment on FWHM to com-

TABLE 2
Uptake Constants Estimated by the Profile and Multiple ROI Methods from Simulated Striatum of Various Uptake Levels

Filter	Profile				Multiple ROI			
	Shepp 1	Hann 1	Hann 0.7	Hann 0.5	Shepp 1	Hann 1	Hann 0.7	Hann 0.5
C_p (6)*	5.76[†] (0.35)[‡]	5.73 (0.26)	5.77 (0.21)	5.75 (0.24)	5.74 (0.27)	5.78 (0.22)	5.84 (0.19)	6.00 (0.15)
C_b (1)	0.96 (0.05)	1.01 (0.08)	1.03 (0.07)	1.04 (0.07)	1.16 (0.08)	1.21 (0.02)	1.23 (0.04)	1.23 (0.05)
width (1.15)	1.28 (0.06)	1.25 (0.04)	1.23 (0.04)	1.21 (0.06)	1.29 (0.08)	1.24 (0.04)	1.19 (0.03)	1.13 (0.02)
C_p (4)	3.81 (0.29)	3.78 (0.22)	3.79 (0.18)	3.78 (0.20)	3.77 (0.22)	3.81 (0.19)	3.86 (0.17)	3.99 (0.15)
C_b (1)	0.94 (0.04)	0.99 (0.06)	1.00 (0.06)	1.01 (0.06)	1.07 (0.07)	1.11 (0.01)	1.14 (0.04)	1.14 (0.04)
width (1.15)	1.34 (0.08)	1.32 (0.06)	1.28 (0.06)	1.26 (0.10)	1.36 (0.18)	1.28 (0.10)	1.22 (0.08)	1.13 (0.06)
C_p (3)	2.86 (0.27)	2.82 (0.22)	2.81 (0.18)	2.80 (0.20)	2.79 (0.22)	2.82 (0.19)	2.87 (0.17)	2.98 (0.15)
C_b (1)	0.95 (0.04)	0.98 (0.06)	0.99 (0.06)	1.00 (0.06)	1.03 (0.07)	1.06 (0.01)	1.09 (0.04)	1.10 (0.04)
width (1.15)	1.40 (0.12)	1.40 (0.11)	1.37 (0.10)	1.33 (0.13)	1.43 (0.18)	1.34 (0.10)	1.25 (0.08)	1.14 (0.06)
C_p (2)	1.90 (0.28)	1.86 (0.20)	1.85 (0.17)	1.84 (0.17)	1.84 (0.18)	1.86 (0.17)	1.90 (0.15)	2.00 (0.14)
C_b (1)	0.90 (0.02)	0.95 (0.05)	0.97 (0.06)	0.98 (0.06)	0.98 (0.06)	1.00 (0.01)	1.04 (0.04)	1.05 (0.04)
width (1.15)	1.81 (0.64)	1.70 (0.34)	1.63 (0.28)	1.53 (0.28)	1.66 (0.35)	1.52 (0.22)	1.34 (0.18)	1.14 (0.35)

*Numbers in parentheses represent true values.
[†]Numbers represent the averages of five noise realizations. The results from image contrast of 6 (C_p = 6) are also shown in Figure 5.
[‡]Numbers represent the averages of standard errors in the estimate.

pensate for deviations from the basic assumption is a function of both image resolution and structural shape.

FWHM adjustments for the multiple ROI method are larger than those of the profile method. This is mainly due to the use of elliptical ROIs that deviate from the theory of assuming rectangular ROIs and partly due to the more averaging by the multiple ROI method of data along the length direction of the putamen. The larger adjustment required at a lower resolution is primarily due to the more pronounced two-dimensional spillover from the surrounding activity (i.e., more deviation from the assump-

tion of an infinite long bar). However, dependency of the adjustment amount on structural shape is not particularly strong (mostly less than 0.5 mm). The effect of using a slightly different FWHM ($\pm$ 1 mm) on the estimated C_p and w has also been evaluated based on the noise-free data of the simulated striata (Table 4). The effects on C_p and w estimates were found to be inversely coupled and were reasonably small except at low imaging resolutions. The effect of adjusting FWHM on the C_b estimate is generally small. Figures 5 and 9 show that the C_p or $(K_3)_{putamen}$ estimates from the profile and multiple ROI methods are independent of image resolution for both
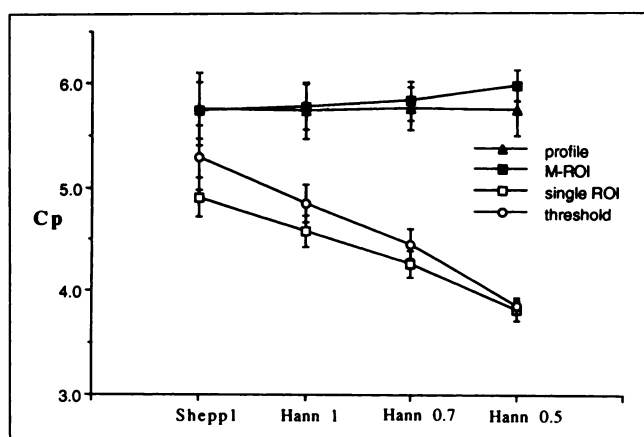

FIGURE 6. C_p estimates by different quantitation methods from noise-added simulated data: profile (triangle), multiple ROI (square), single ROI (unfilled square) and 15% thresholding (open circle). C_p estimates from the single ROI and thresholding methods are strongly dependent on image resolution and are much lower than the true value of 6. The error bars are the standard deviation of the corresponding estimates in five noise realizations.
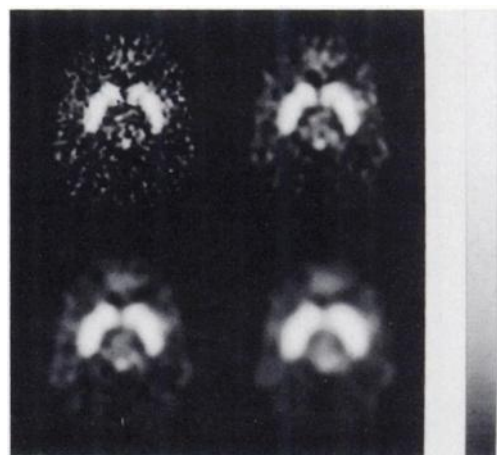

FIGURE 7. Parametric images of the FDOPA uptake constant at four different resolutions [upper left: Shepp 1; upper right: Hann 1; lower left: Hann 0.7; lower right: Hann 0.5)] from a PET study of a normal subject (see text for procedure to generate parametric images). The gray scale of each image was normalized to the maximal value of that image.

simulation and PET data, except for the small dependency of the $(K_3)_{putamen}$ estimates with the profile method. Because the FWHM from computer simulations was directly applied to the PET studies, some physical factors (such as scattering and nonuniform sampling) and anatomical factors (such as structural shape differences of the putamen) were not accounted for and may thus explain the small decrease of the $(K_3)_{putamen}$ estimate with a decreasing FWHM.

Axial positioning of the putamen relative to the image plane is another important issue. The axial dimension of the putamen in a normal subject is about 2.0–2.5 cm, which is relatively long compared to the axial resolution (7 mm) of the PET scanner used in this study (25). Since only the cross-sectional plane that intersected the middle of the putamen was selected for analysis, the assumption of negligible variation along the axial direction should be an acceptable approximation. Possible error due to orientation of the putamen was also tested. When the simulated putamen was tilted sideways by 8 degrees axially, a 3.2% decrease for the profile method and a 2.5% decrease for the multiple ROI method were observed in the C_p estimate. An additional tilt of 8 degrees gave 11% and 8% changes in C_p estimates for the profile and multiple
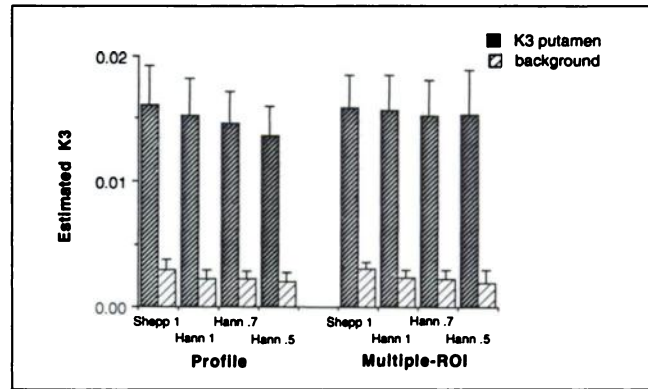
FIGURE 9. Estimates of $(K_3)_{putamen}$ and $(K_3)_{background}$ from normal human studies at four image resolutions. The error bars are the standard deviations of the estimates of five normal subjects.

ROI methods, respectively. The result implies that small variations in structural shape in the axial direction or non-abrupt activity transition between object and background is not expected to significantly affect the C_p estimate. Although we only considered two-dimensional activity distribution in this study, the multiple ROI and profile methods can potentially be extended to account for three-dimensional configurations of a structure to further improve quantitation.

Structures other than the putamen and caudate also have specific FDOPA uptake and contribute to the background level in parametric images (Fig. 7). Background uptake implies that the correction method using a simple recovery coefficient for the measured activity might be incorrect for FDOPA studies because the spillover from surrounding tissue to the putamen should not be corrected by the recovery coefficient. By including background uptake as a variable parameter, the present methods can properly account for non-zero background. However, due to nonuniformity of background in FDOPA images, the profile and background levels should not be extended too far.

Parametric images give FDOPA uptake constants on a pixel-by-pixel basis, which allows clearer examination of the functional parameter's spatial distribution. In this study, Patlak analysis was used to generate parametric images of FDOPA uptake constant. This analytic approach has been used previously for PET FDOPA studies (2,26). With the use of the cerebellum as the reference region, the uptake constant was shown to correlate well with the uptake constant calculated from a model approach (4). Although other regions may be used as a reference (3,27) for measured activity from OMFD, no significant effect on the results is expected because OMFD distributes uniformly over all brain regions (28). Although Patlak analysis was used to generate the uptake constant K_3, the assumption of an irreversible uptake of tracer is not rigorously valid for FDOPA in striatal tissue
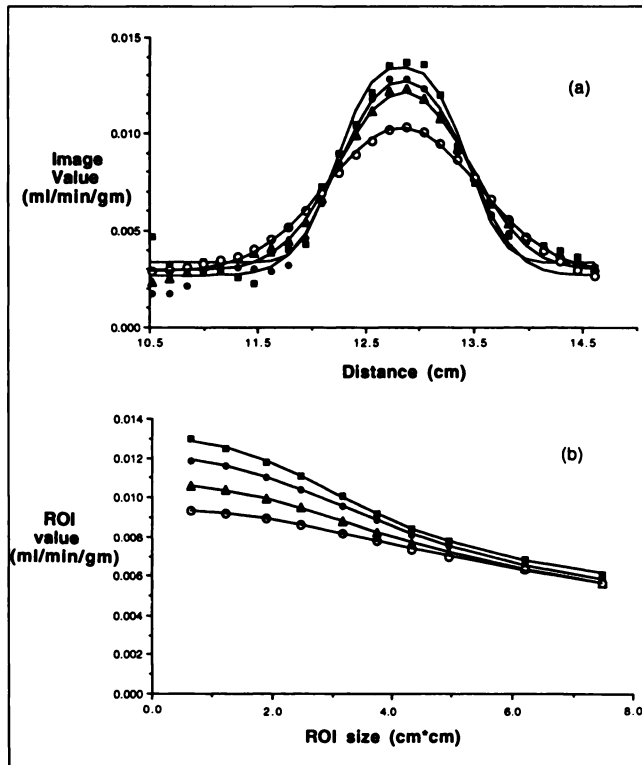

FIGURE 8. (a) Profiles across the putamen of a normal study. The symbols and curves represent, respectively, the measured values and their fitting results from Equation 1 at four image resolutions (square: Shepp 1; circle: Hann 1; triangle: Hann 0.7; open circle: Hann 0.5). (b) Measured ROI values and fitting results from Equation 2 for image resolutions in Figure 7.

TABLE 3
Percent Changes of Estimated Uptake Constants for Misplaced ROIs and Profiles

| | Profile | Multiple ROI | | | |
	Location moves down 0.8 cm	Center shifts 0.157 cm	Center shifts 0.314 cm	Dimension increases 40%	Dimension decreases 40%
$(K_3)_{putamen}$ (ml/min/g)	11.6 ($\pm$11.7)*	−7.0 ($\pm$9.8)	−27.7 ($\pm$12.1)	−5.7 ($\pm$5.2)	6.5 ($\pm$28.1)
$(K_3)_{background}$ (ml/min/g)	−19.3 ($\pm$42.4)	19.2 ($\pm$8.7)	46.1 ($\pm$25.3)	−7.4 ($\pm$15.3)	7.9 ($\pm$22.4)
Width (cm)	−9.6 ($\pm$13.0)	−0.5 ($\pm$12.5)	12.7 ($\pm$28.8)	−2.5 ($\pm$8.2)	−3.1 ($\pm$20.1)

*Standard deviation of the percent change for the left and right putamens of FDOPA studies in five normal subjects.

(4). However, the clearance rate estimate (k_4) of FDOPA and its metabolites from striatal tissue has not been found to vary much in normals and in most disease states (4,26). In these situations, the effect of assuming a zero k_4 on the estimated K_3 value is predictable and correctable (26). In other words, the use of Patlak analysis for generating K_3 parametric images is not expected to impose any severe practical limitation.

Patients with Parkinson's disease have reduced uptake of FDOPA and hence lowered contrast between the putamen and its background (31). For studies with a putamen-to-background contrast as low as 2:1, the results shown in Table 2 indicate that the accuracy of the estimated C_p and C_b for the two proposed quantitation methods are not significantly affected by the low contrast, though the width is apparently overestimated. On the other hand, when the putamen-to-background contrast is extremely low, the spillover loss of activity from putamen-to-background would not be as significant, and the single ROI method is quite adequate for giving reliable results.

Errors in neighboring pixels in the reconstructed PET image are correlated (32), whereas least-square fitting assumes independent noise. Usually, ignoring the noise correlation in the estimation does not cause any significant bias in the estimates, as shown by the results in the

present study. However, the estimates may not be optimal, especially in the case of high noise level and low contrast. The small bias shown in Figure 5 is believed to be due to noise correlation in the image. In such cases, the use of more sophisticated methods (33–35) that account for noise correlation may potentially improve the results.

For the multiple ROI method, a dimensional change of the ROI size by 40% and a miscentering by one pixel had no significant effect on the K_3 estimate. The large standard deviation for the decreased dimension of ROI (Table 3) is believed to be due to high statistical noise of smaller ROIs. Results estimated from the profile method are not sensitive to change in the profile location for all four image resolutions as long as the profile is within the middle 1-cm section of the putamen. The estimated width decreases as the profile location moves posteriorly. This is consistent with tapering the physical size of the putamen in the posterior side. The estimate of $(K_3)_{background}$ varies significantly as the location of the profile is changed. This is probably due to the influence of higher image values in such adjacent tissue structures as the thalamus and caudate that are near the medial-posterior and anterior sides of the putamen. The relative insensitivity of the estimates for placement of ROIs and locating profiles and the resolution independence of the two

TABLE 4
Percent Change of C_p and Width Estimates due to Inaccurate FWHM

| Reconstruction filter | Profile | | Multiple ROI | |
	FWHM − 1mm‡	FWHM + 1mm‡	FWHM − 1mm	FWHM + 1mm
Shepp 1	−5*/+4†	+5/−3	−3/+2.6	+4/−1
Hann 1	−7/+6	+8/−9	−5/+3.4	+8/−8
Hann 0.7	−9/+8	+13/−15	−9/+6.1	+13/−15
Hann 0.5	−12/+14	+21/−23	−12/+13	+33/−31

*Percent change of the estimated C_p from its true value.
†Percent change of the estimated structural width from its true value.
‡FWHM in the fitting equations was adjusted by a magnitude of −1 of +1 mm.

quantitation methods indicate that they are usable for estimating $(K_3)_{putamen}$ for cross-comparison of results from different laboratories or investigators. The only questionable issue is that these methods appear to give a larger variability (about 1.5 times of that of the single ROI method), particularly at the lowest resolution (its coefficient of variation is 2.5 times of that of the single ROI method), mainly because the assumption of one-dimensional variation is no longer a good assumption at such a low resolution. Also, the coefficient of variation for the single ROI method is expected to be larger if the ROIs were defined individually on each image. The intersubject variability of PET data and subjectivity in defining ROIs make objective comparison more difficult.

The major advantage of the profile and multiple ROI methods over conventional methods is that they account for image resolution. As shown in Figure 6, the C_p value from the conventional methods are underestimated and have a larger variation across different resolutions, while the present methods give results closer to the true activity and are not affected by image resolution. A comparison of estimates from different methods indicates a good correlation between the present methods and the single ROI method (c.c. = 0.82–0.95) for data from five normal subjects. This implies that no significant amount of additional error was introduced when applying the profile and multiple ROI methods. Results in this study indicate that these methods have definite advantages over conventional method for cases of moderate and high spatial resolution (FWHM < width of structure). However, if FWHM resolution is larger than the structural width or the striatum-to-background contrast is low ($\leq$ 2.0), or there is significant deviation from the uniform activity assumption for the striatum and the background, the conventional method probably should be used and partial volume effect should not be corrected.

These two methods have comparable performance in terms of accuracy and error sensitivity (Fig. 6, Tables 3, 4) for most situations. However, for images of higher noise condition, the multiple ROI method is expected to give more stable results because more pixels are used. For studies that require both accurate estimation of structural width and background uptake, the profile method is more appropriate. Regardless of the method used, correcting for partial volume effect in images at very low resolutions becomes more difficult because the putamen and caudate activities are not distinguishable and the imaged activity is a mixture of activities from the putamen, caudate and internal capsule (tissue between the caudate and putamen).

Based on the one-dimensional simplified model, these methods can account for background uptake and provide FDOPA uptake rate constants that are independent of image resolution. The implementation of these two methods for routine use is relatively simple and no data from other imaging modalities are required. Although the

structure of the putamen and FDOPA uptake do not rigorously satisfy all the assumptions stated in the theory section, they are reasonable approximations that allow the application of Equations 1 and 2 to the FDOPA data. For application of these two methods to other structures of grossly different shape, modifications may be needed and the accuracy needs to be carefully assessed. These proposed quantitation methods, which can estimate the structural activity level, background level and size simultaneously, are expected to be useful for improving the quantitative results of FDOPA PET studies.

ACKNOWLEDGMENTS

REFERENCES

1. Garnett ES, Firnau G, Nahmias C. Dopamine visualized in the basal ganglia of living man. *Nature* 1983;305:137–138.
2. Martin WRW, Palmer MR, Patlak CS, Calne DB. Nigrostriatal function in humans studied with positron emission tomography. *Ann Neurol* 1989;26:535–542.
3. Gjedde A, Reith J, Dyve S, Leger G, Guttman M, Diksic M. Dopa decarboxylase activity of the lovong human brain. *Proc Natl Acad Sci* 1991;88:2721–2725.
4. Huang SC, Yu DC, Grafton S, Melega WP. Kinetics and modeling of 6-[F-18]Fluoro-L-dopa in human positron emission tomography studies. *J Cereb Blood Flow Metabol* 1991;11:898–913.
5. Barrio JR, Huang SC, Phelps ME. In vivo assessment of neurotransmitter biochemistry in humans. *Ann Rev Pharmacol Toxicol* 1988;28:213–230.
6. Calne DB, Langston JW, Martin WRW, et al. Positron emission tomography after MPTP: observations relating to the cause of Parkinson's disease. *Nature* 1985;317:246–248.
7. Martin WRW, Stoessl AJ, Adam MJ, et al. Positron emission tomography in Parkinson's disease: glucose and dopa metabolism. *Adv Neurol* 1986;45:95–98.
8. Leenders KL, Palmer AJ, Quinn N, et al. Brain dopamine metabolism in patients with Parkinson's disease measured with positron emission tomography. *J Neurol Neurosurg Psychiatry* 1986;49:853–860.
9. Leenders KL, Aquilonius S-M, Bergstrom K, et al. Unilateral MPTP lesion in a rhesus monkey: effects on the striatal dopaminergic system measured in vivo with PET using various novel tracers. *Brain Rev* 1988;445:61–67.
10. Melega WP, Hoffman JM, Schneider JS, Phelps ME, Barrio JR. 6-[F-18]fluoro-L-dopa metabolism in MPTP-treated monkeys: assessment of tracer methodologies for positron emission tomography. *Brain Res* 1991;543:271–276.
11. Boyes BE, Cumming P, Martin WRW, McGeer EG. Determination of plasma [F-18]-6-fluorodopa during positron emission tomography: elimination and metabolism in carbidopa treated subjects. *Life Sci* 1986;39:2243–2252.
12. Patlak CS, Blasberg RG, Fenstermacher JD. Graphical evaluation of blood-to-brain transfer constants from multiple-time uptake data. *J Cereb Blood Flow Metab* 1983;3:1–7.
13. Patlak CS, Blasberg RG. Graphical evaluation of blood-to-brain transfer constants from multiple-time uptake data. *J Cereb Blood Flow Metab* 1985;5:584–590.
14. Mazziotta JC, Phelps ME, Plummer D, Kuhl DE. Quantitation in positron

emission computered tomography: 5. Physical-anatomical effects. *J Comput Assist Tomogr* 1981;5:734–743.

15. Bendriem B, Dewey SL, Schlyer DJ, Wolf AP, Volkow ND. Quantitation of the human basal ganglia with positron emission tomography: a phantom study of the effect of contrast and axial positioning. *IEEE Trans Med Imag* 1991;5:203–213.

16. Hoffman EJ, Huang SC, Phelps ME. Quantitation in positron emission computed tomography. 1. Effect of object size. *J Comput Assist Tomogr* 1979;3:299–308.

17. Kessler R, Ellis JR, Eden M. Analysis of emission tomography scan data: limitations composed by resolution and background. *J Comput Assist Tomogr* 1984;8:514–522.

18. Gjedde A, Reith J, Kuwabara H, Dyve S. Determining dopa decarboxylase activity in the human brain in vivo: the complete fluoro-dopa model. *J Nucl Med* 1990;31:720.

19. Eidelberg D, Moeller JR, Dhawan V, et al. The metabolic anatomy of Parkinson's disease complementary [F-18]fluorodeoxyglucose and [F-18]fluorodopa positron emission tomography studies. *Movement Disorder* 1990;5:203–213.

20. Rottenberg DA, Moeller JR, Strother SC, Dhawan V, Sergi ML. Effects of percent thresholding on the extraction of [F18]fluorodeoxyglucose positron emission tomographic region-of-interest. *J Cereb Flow Metab* 1991;11:A83–A88.

21. Gambhir SS. Quantitation of the physical factors affecting tracer kinetic modeling of cardiac positron emission tomography data, PhD Dissertation Thesis, University of California, Los Angeles; 1991.

22. Abramowitz M, Stegun IA. *Handbook of mathematical functions.* New York: McGraw-Hill; 1972.

23. Huang SC, Carson RE, Phelps ME, Hoffman EJ, Schelbert HR, Kuhl DE. A boundary method for attenuation correction in positron computed tomography. *J Nucl Med* 1981;22:627–637.

24. Carson RE, Huang SC, Phelps ME. BLD: a software system for physi-

ological data handling and model analysis. *The 5th Annual Symposium on Computer Applications in Medical Care* 1981;562–565.

25. Miller TM, Wallis JW, Grothe RA Jr. Design and use of PET tomography: the effect of slice spacing. *J Nucl Med* 1990;31:1732–1739.

26. Yu DC, Huang SC, Melega WP, et al. Evaluation of various graphical analysis for estimating influx constant in F-DOPA PET studies. *J Nucl Med* 1991;32 suppl:1004.

27. Pate BD, Snow BJ, Hewitt KA, Morrison KS, Ruth TJ, Calne DB. The reproducibility of striatal uptake data obtained with positron emission tomography and fluorine-18-L-6-fluorodopa tracer in nonhuman primates. *J Nucl Med* 1991;32:1246–1251.

28. Doudet DJ, McLellan CA, Carson RE, et al. Distribution and kinetics of 3-O-methyl-6-[F-18]fluoro-L-DOPA in the Rhesus monkey brain. *J Cereb Blood Flow Metab* 1991;11:726–734.

29. Gambhir SS, Schwaiger M, Huang SC, et al. Simple noninvasive quantification method for measuring myocardial glucose utilization in human employing positron emission tomography and fluorine-18-deoxyglucose. *J Nucl Med* 1989;30:359–366.

30. Choi Y, Hawkins RA, Huang SC, et al. Parametric images of myocardial metabolic rate of glucose generated from dynamic cardiac PET and 2-[^{18}F]fluoro-2-deoxy-d-glucose studies. *J Nucl Med* 1991;32:733–738.

31. Brooks DJ, Ibanez V, Sawle GV, et al. Differing pattern of striatal ^{18}F-dopa uptake in Parkinson's disease, multiple system atrophy and progressive supranuclear palsy. *Ann Neurol* 1990;28:547–555.

32. Kak AC, Slaney M. *Principles of computerized tomographic imaging.* New York: IEEE Press; 1987.

33. Huesman RH, Mazoyer BM. Kinetic data analysis with a noisy input function. *Phys Med Biol* 1987;32:1569–1579.

34. Chen K, Huang SC, Yu DC. The effect of measurement errors in the plasma radioactivity curve on parameter estimation in positron emission tomography. *Phys Med Biol* 1991;36:1183–1200.

35. Draper NR, Smith H. *Applied regression analysis,* 2nd edition. New York: Wiley; 1981.

SELF-STUDY TEST
Gastrointestinal Nuclear Medicine

Questions are taken from the *Nuclear Medicine Self-Study Program 1*,
published by The Society of Nuclear Medicine

DIRECTIONS

The following items consist of a heading followed by lettered options related to that heading. Select the one lettered option that is best for each item. Answers may be found on page 694.

True statements concerning scintigraphy for detection of Meckel's diverticulum include which of the following?

1. Pretreatment with cimetidine increases the frequency of false-negative studies.
2. Uterine blood-pool activity occasionally causes false-positive studies.
3. Small bowel duplication is usually distinguishable from Meckel's diverticulum.
4. Technetium-99m pertechnetate is selectively concentrated in parietal cells of ectopic gastric mucosa.

True statements regarding Meckel's diverticula in adults include which of the following?

5. Most are symptomatic.
6. Two-thirds of affected elderly patients present with melena.
7. Technetium-99m pertechnetate imaging has a sensitivity of greater than 80%.

A 35-year-old man was admitted with abdominal pain, melena, and orthostatic hypotension. Upper gastrointestinal endoscopy to the second portion of the duodenum was normal. Melena persisted and the patient required multiple transfusions. Colonoscopy to the hepatic flexure demonstrated melena, but no actively bleeding lesion. The colono-

scope could not be advanced further because of spasm. Scintigraphy with ^{99m}Tc-labeled red blood cells was performed (Fig. 1). Images were taken at 5, 10, 15, and 20 minutes.
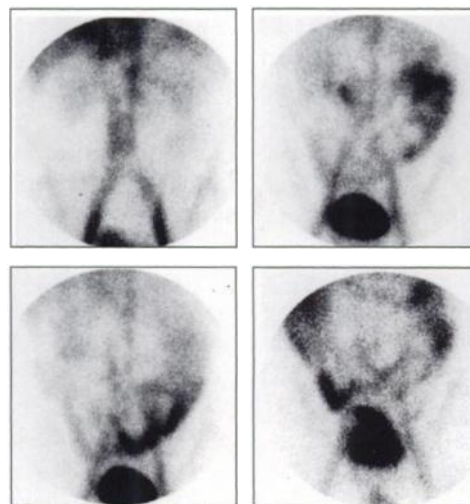

Figure 1